

# Measuring the Weak Mixing Angle in the DUNE Near Detector Complex

André de Gouvêa,<sup>1</sup> Pedro A. N. Machado,<sup>2</sup> Yuber F. Perez-Gonzalez,<sup>1,2,3</sup> and Zahra Tabrizi<sup>4</sup>

<sup>1</sup>*Department of Physics & Astronomy, Northwestern University, Evanston, IL 60208, USA*

<sup>2</sup>*Theoretical Physics Department, Fermilab, P.O. Box 500, Batavia, IL 60510, USA*

<sup>3</sup>*Colegio de Física Fundamental e Interdisciplinaria de las Américas (COFI),  
254 Norzagaray street, San Juan, Puerto Rico 00901*

<sup>4</sup>*Instituto de Física Gleb Wataghin, Universidade Estadual de Campinas (UNICAMP),  
Rua Sérgio Buarque de Holanda, 777, Campinas, SP, 13083-859, Brazil*

The planned DUNE experiment will have excellent sensitivity to the vector and axial couplings of the electron to the  $Z$ -boson via precision measurements of neutrino–electron scattering. We investigate the sensitivity of DUNE-PRISM, a movable near detector in the direction perpendicular to the beam line, and find that it will qualitatively impact our ability to constrain the weak couplings of the electron. We translate these neutrino–electron scattering measurements into a determination of the weak mixing angle at low scales and estimate that, with seven years of data taking, the DUNE near-detector can be used to measure  $\sin^2\theta_W$  with better than 2% precision. We also discuss the impact of combining neutrino–electron scattering data with neutrino trident production at DUNE-PRISM.

The standard model of particle physics (SM) is a relativistic quantum field theory characterized by an  $SU(3)_c \times SU(2)_L \times U(1)_Y$  gauge symmetry, corresponding to the color, weak-isospin and hypercharge interactions, respectively, along with a set of fermion and boson fields which describe the elementary particles observed in nature. Free SM parameters – the gauge couplings, the Yukawa couplings, and the parameters of the scalar potential – need to be determined by comparing the results of theoretical computations to a finite set of the experimental measurements.

The weak mixing angle  $\theta_W$  (or, more precisely, its sine-squared,  $\sin^2\theta_W$ ) parameterizes several measurable quantities, including the ratio of the masses of the weak gauge bosons, several weak-interaction cross sections, and parity-violating observables. It is a crucial ingredient of the *electroweak precision observables*, a set of experimental observables designed to test the internal consistency of the SM.

The exact definition of the weak mixing angle depends on the renormalization scheme, that is, the convention of which quantities are taken as input and which are derived from these inputs, along with the recipe for handling quantum corrections. As quantum corrections are relevant,  $\sin^2\theta_W$  depends on the scale at which it is being measured. For example, in the modified minimal subtraction scheme [1, 2],  $\overline{\text{MS}}$ , the weak mixing angle is defined in terms of the weak gauge couplings

$$\sin^2\theta_W(\mu) \equiv \frac{g'^2(\mu)}{g^2(\mu) + g'^2(\mu)}, \quad (1)$$

where  $g$  and  $g'$  are the coupling constants of  $SU(2)_L$  and  $U(1)_Y$ , respectively, and  $\mu$  is the scale of the physical process under consideration. The SM predicts, under a specific renormalization scheme, a unique scale dependence for  $\sin^2\theta_W$ . This dependence has been confirmed by precise measurements at very different en-

ergy scales, including atomic parity violation, electron-proton scattering, Möller scattering, neutrino–nucleus and neutrino–electron scattering, electron deep-inelastic scattering, and the  $Z$ - and  $W$ -boson masses (see Ref. [3] for a comprehensive review).

The NuTeV result [4], the most precise measurement of  $\sin^2\theta_W$  using neutrino scattering, stands out from the other measurements. Making use of measurements of the ratios of neutral to charged-current and neutrino–nucleus to antineutrino–nucleus cross sections, they find  $\sin^2\theta_W = 0.2407 \pm 0.0016$  (in the  $\overline{\text{MS}}$  scheme) at an average energy scale  $\langle\mu\rangle \simeq 4.5$  GeV. This measurement deviates from the SM expectation anchored by the more precise measurements at LEP [5] at the  $3\sigma$  level. Effects inherent to the intricacies of neutrino-nucleus scattering, potentially unaccounted for or only partially accounted for by the collaboration, have been identified as candidate sources for the discrepancy [6–24]. A definitive answer remains elusive. Regardless, it stands to reason that other precise measurements of  $\sin^2\theta_W$  using neutrino scattering will help shed light on the situation.

Next-generation neutrino experiments like LBNF-DUNE [25] and T2HK [26] include very intense neutrino beams with energies that range from several hundred MeV to several GeV. The neutrino–nucleus scattering cross sections, at these energies, have large uncertainties due to nuclear and non-perturbative effects [27], making it very challenging to use them to infer  $\sin^2\theta_W$ . Neutrino–electron scattering, on the other hand, provides a more promising environment for precision measurements [28–32]. Even in this case, however, one still needs to address significant challenges. First, the cross section for neutrino–electron scattering is three orders of magnitude smaller than that for neutrino-nucleus scattering, translating into poor statistics in most neutrino experiments. Second, while the neutrino–electron cross section depends mostly on  $\sin^2\theta_W$  plus very small elec-

troweak corrections [33, 34], the neutrino beam originates from the in-flight decay of charged mesons, mostly pions and kaons, produced when high-energy protons hit a fixed target. First-principles computations of the meson production rate and kinematics are not possible and one must rely on phenomenological models and experimental data; uncertainties on the overall neutrino flux and energy distribution are at the 5% to 15% level [35–37].

Near detector complexes are designed to circumvent some of the large uncertainties in the neutrino flux and the neutrino–nucleus cross sections and allow precision measurements of neutrino oscillations. These are expected to collect huge samples of neutrino scattering events. DUNE-PRISM [38], currently part of the LBNF-DUNE proposal, is a near detector that is capable of moving in the direction perpendicular to the neutrino-beam axis. Although the neutrino flux has prohibitively large uncertainties, the ratios of on-axis to off-axis fluxes are dictated only by meson-decay kinematics and thus are much better understood. Therefore, measurements of the neutrino–electron–scattering spectrum at different off-axis positions should allow an unprecedented measurement of the weak mixing angle with neutrinos.

In general terms, the neutrino–electron scattering cross-section depends on the vector and axial couplings,  $g_V$  and  $g_A$ , between the  $Z$ -boson and the electron (see measurements performed by CHARM-II [39], LSND [40] and TEXONO [41]). We will estimate the DUNE-PRISM sensitivity to such parameters via neutrino–electron scattering data. A hidden but very safe assumption is that the cross-section depends only on the left-handed coupling of the neutrino to the  $Z$ -boson. The reason for this is that all neutrinos and antineutrinos used in neutrino scattering are produced in charged-current processes ( $\pi^+ \rightarrow \mu^+ \nu_\mu$ ,  $n \rightarrow p e \bar{\nu}_e$ ,  $D_s \rightarrow \tau^+ \nu_\tau$ , etc) and are, to a very good precision, 100% polarized. We will assume this is the case throughout. Lepton-collider data, combined with those from neutrino–electron scattering, for example, can be used to determine the right-handed-coupling of neutrinos to the  $Z$ -boson [42].

The differential cross section for a neutrino with flavor  $\alpha = e, \mu, \tau$  to scatter off an electron at rest is

$$\begin{aligned} \frac{d\sigma}{dE_R} &= \frac{2G_F^2 m_e}{\pi} \left\{ g_1^2 + g_2^2 \left( 1 - \frac{E_R}{E_\nu} \right)^2 - g_1 g_2 \frac{m_e E_R}{E_\nu^2} \right\} \\ &\simeq 1.72 \times 10^{-41} \left\{ g_1^2 + g_2^2 \left( 1 - \frac{E_R}{E_\nu} \right)^2 \right\} \frac{\text{cm}^2}{\text{GeV}}, \quad (2) \end{aligned}$$

where  $G_F$  is the Fermi constant,  $E_\nu$  is the incoming neutrino energy, and  $m_e$  and  $E_R$  are the electron mass and recoil kinetic energy, respectively.

The couplings  $g_1$  and  $g_2$  depend on the neutrino flavor and can be written in terms of the electron vector and axial couplings to the  $Z$ -boson,  $g_V$  and  $g_A$ , as listed in Table I. Assuming the SM, these can be expressed in

terms of  $\sin^2 \theta_W$ . More generally, if  $g_V$  and  $g_A$  are considered to be free parameters, they can be independently extracted from the recoil-electron energy spectrum so data from DUNE-PRISM are expected to constrain nontrivial regions in the  $g_V \times g_A$  plane.

TABLE I. Couplings  $g_1$  and  $g_2$  (see Eq. (2)) as a function of the electron– $Z$ -boson couplings  $g_V$  and  $g_A$ , for each neutrino flavor, along with the corresponding SM value.  $s_W^2 \equiv \sin^2 \theta_W$ .

$\nu_\alpha$	$g_1$	$g_1(\text{SM})$	$g_2$	$g_2(\text{SM})$
$\nu_e$	$1 + (g_V + g_A)/2$	$1/2 + s_W^2$	$(g_V - g_A)/2$	$s_W^2$
$\nu_{\mu,\tau}$	$(g_V + g_A)/2$	$-1/2 + s_W^2$	$(g_V - g_A)/2$	$s_W^2$
$\bar{\nu}_e$	$(g_V - g_A)/2$	$s_W^2$	$1 + (g_V + g_A)/2$	$1/2 + s_W^2$
$\bar{\nu}_{\mu,\tau}$	$(g_V - g_A)/2$	$s_W^2$	$(g_V + g_A)/2$	$-1/2 + s_W^2$

Strictly speaking, the neutrino–electron cross section is also subject to quantum corrections that will introduce additional dependence on  $Q^2 \equiv 2E_R m_e$  [33, 34]. Kinematics dictates that the maximum recoil energy is approximately  $E_R^{\text{max}} \simeq E_\nu - m_e/2$ . Due to kinematics and the energy profile of DUNE’s neutrino flux, most electron recoil events will lie within  $0.2 \lesssim E_R \lesssim 10$  GeV. Therefore, the  $Q^2$  values accessible to DUNE are, roughly, in the range  $(10 - 100 \text{ MeV})^2$ , where loop corrections to  $\sin^2 \theta_W$  have little scale dependence [3]. In view of this, by analyzing the  $Q^2$  distribution in detail, the couplings in Eq. (2) can be interpreted as the renormalized couplings in the  $\overline{\text{MS}}$  scheme at an average scale  $\langle Q^2 \rangle = (40 \text{ MeV})^2$ .

Assuming the SM, the cross section for  $\nu_\mu - e$ -scattering is

$$\frac{d\sigma}{dE_R} \propto \left( \frac{1}{4} - \sin^2 \theta_W \right) + \sin^4 \theta_W \left( 2 - \frac{2E_R}{E_\nu} + \frac{E_R^2}{E_\nu^2} \right). \quad (3)$$

Since  $\sin^2 \theta_W$  is close to  $1/4$ , the first term is suppressed relative to the second one. This implies that the value of  $\sin^2 \theta_W$ , to leading order, modifies the overall normalization of the  $\nu_\mu - e$ -scattering cross section and the effect of changing  $\sin^2 \theta_W$  is nearly degenerate with that of changing the overall normalization of the  $\nu_\mu$  flux. A similar argument applies to  $\bar{\nu}_\mu - e$ -scattering. The situation is different for  $\nu_e - e$  and  $\bar{\nu}_e - e$  scattering;  $\sin^2 \theta_W$  has a significant impact on the shape of the recoil-electron energy distributions. It turns out, unfortunately, that, at DUNE, the neutrino flux is dominated by  $\nu_\mu$  and the  $\nu_e$  contribution is relatively small, around a few percent.

In this context, DUNE-PRISM is expected to provide nontrivial information. In accelerator neutrino experiments, the  $\nu_\mu$  comes predominantly from the two-body decay  $\pi^+ \rightarrow \mu^+ \nu_\mu$  (and  $K^+ \rightarrow \mu^+ \nu_\mu$ , to a lesser extent) while the  $\nu_e$  comes from the three-body decays of kaons and muons. For the same parent energy, the flux of  $\nu_e$

has a larger angular spread than that of  $\nu_\mu$  so the off-axis  $\nu_e$  to  $\nu_\mu$  flux ratio is larger than the on-axis one.

To estimate and put in context how well DUNE-PRISM can contribute to the precision electroweak physics program, we will compute the DUNE sensitivity to  $\sin^2 \theta_W$  for both on-axis and off-axis runnings. For concreteness, we will assume seven years of data taking equally divided between neutrino and antineutrino modes. We assume a 75 ton fiducial mass liquid argon time projection chamber (LArTPC) and a 1.2 MW proton beam, as described in the DUNE Conceptual Design Report [25]. For the off-axis configuration, we assume the near detector will take data at seven different positions, one year in each configuration. The detector is assumed to be 574 m away from the source in the beam axis direction while its transverse distances to the beam axis are  $6N$  meters,  $N = 0, \dots, 6$ . The detector experiences at each position a flux that is approximately  $10N$  mrad off-axis, respectively. Fig. 1 depicts the ratio of the number of events expected from  $\nu_e - e$  and  $\bar{\nu}_e - e$ -scattering to that of  $\nu_\mu - e$ -scattering, in neutrino-mode running, as a function of the off-axis distance. As expected, the relevance of the  $\nu_e$  and  $\bar{\nu}_e$ -initiated events grows significantly with the off-axis angle. Note that, while the flux ratio is of order a few percent, the  $\nu_e - e$ -scattering cross section is larger than the  $\nu_\mu - e$  so, even on-axis, the  $\nu_e$  contribution is of order 10%.

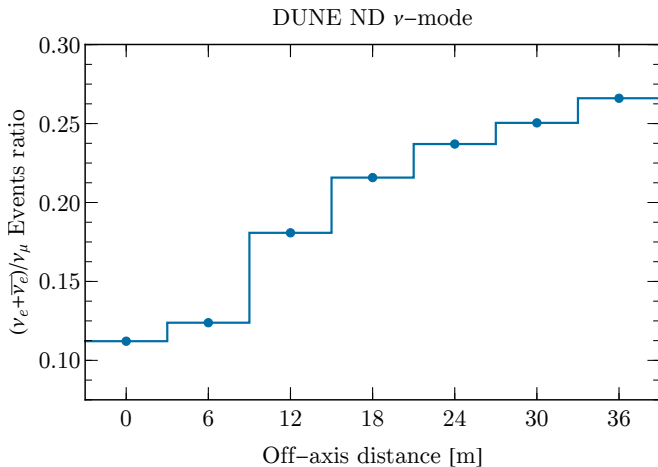


FIG. 1. Ratio of the number of events expected from  $\nu_e - e$  and  $\bar{\nu}_e - e$ -scattering to that of  $\nu_\mu - e$ -scattering, in neutrino-mode running, as a function of the off-axis distance.

To account for the energy-dependent neutrino-flux uncertainties and the correlations between the fluxes at different off-axis angles, we make use of a covariance matrix  $C$ , spanning all DUNE-PRISM positions and neutrino flavors, derived from detailed simulations of hadron production in the beam target followed by magnetic-horn focusing of charged particles [43]. We defined a test statis-

tics

$$\chi^2 = (\mathbf{D} - \mathbf{T})^T C^{-1} (\mathbf{D} - \mathbf{T}), \quad (4)$$

where  $\mathbf{D}$  and  $\mathbf{T}$  are vectors of Asimov data and expectation values, respectively, spanning all positions and bins. The binning is performed in  $E_e \theta_e^2$ , where  $E_e = E_R + m_e$  is the total electron energy and  $\theta_e$  is the scattering angle of the electron relative to the beam direction. We consider a threshold kinetic energy  $E_R > 50$  MeV and perform the analysis in the range  $(0.05 < E_R < 20)$  GeV.

The main background for neutrino-electron scattering is charged-current quasi-elastic (CCQE)  $\nu_e$ -scattering events,  $\nu_e A \rightarrow e^- A'$ . Although the  $\nu_e$  flux is only a few percent of the total neutrino flux, the CCQE cross section is over 1000 times larger than that for neutrino-electron scattering. Kinematics limit the maximum value of  $E_e \theta_e^2$  for neutrino-electron scattering and we adopt the standard cut  $E_e \theta_e^2 < 2m_e$  to improve background rejection. LArTPCs have an exquisite angular resolution, of order  $1^\circ$ , for electromagnetic showers [25]. With all this in mind, we have determined, numerically, that the CCQE background is negligible.

Fig. 2 depicts the DUNE sensitivity to the vector and axial couplings,  $g_V$  and  $g_A$ , in the on-axis LArTPC (dashed green) or the DUNE-PRISM configuration (dark-blue). For comparison, we include existing measurements from CHARM-II [39] (gray), LSND [40] (dotted light-brown) and TEXONO [41] (dot-dashed light-violet). Both the DUNE on-axis and CHARM-II measurements suffer from a four-fold degeneracy; this is a consequence of the fact that the neutrino flux in both these experiments is dominated by  $\nu_\mu$ . There is an exact degeneracy in the differential cross section for  $\nu_\mu - e$  scattering under the transformations

$$(g_V, g_A) \rightarrow (g_A, g_V) \quad \text{and} \quad (g_V, g_A) \rightarrow (-g_V, -g_A), \quad (5)$$

see Eq. (2) and Table I, and hence an experiment with a pure  $\nu_\mu$  beam is intrinsically limited. The TEXONO experiment measured electron recoils from electron antineutrinos produced in a nuclear reactor. The scattering cross section, in this case, is proportional to  $3g_1^2 + g_2^2$ , which defines an oblique ellipse in the  $(g_V, g_A)$  plane centered at  $(-0.5, -0.5)$ . The TEXONO result in Fig. 2 reflects this fact, up to effects related to information on the recoil energy spectrum. The LSND measured can also be understood by using similar arguments, taking into account that the flux of neutrinos at LSND consists of  $\nu_\mu$ ,  $\bar{\nu}_\mu$ , and  $\nu_e$  with well-characterized energy spectra from (mostly) pion decay at rest, followed by muon decay at rest. Current data are not able to rule out very small  $g_A$  and  $g_V \sim -0.5$  (region on the left-hand part of Fig. 2)

In DUNE-PRISM, the presence of both  $\nu_\mu$  and  $\nu_e$ , along with their antiparticles, is a powerful tool for lifting degeneracies without resorting to data from other experiments. To illustrate this point, Fig. 3 depicts the  $E_e \theta_e^2$

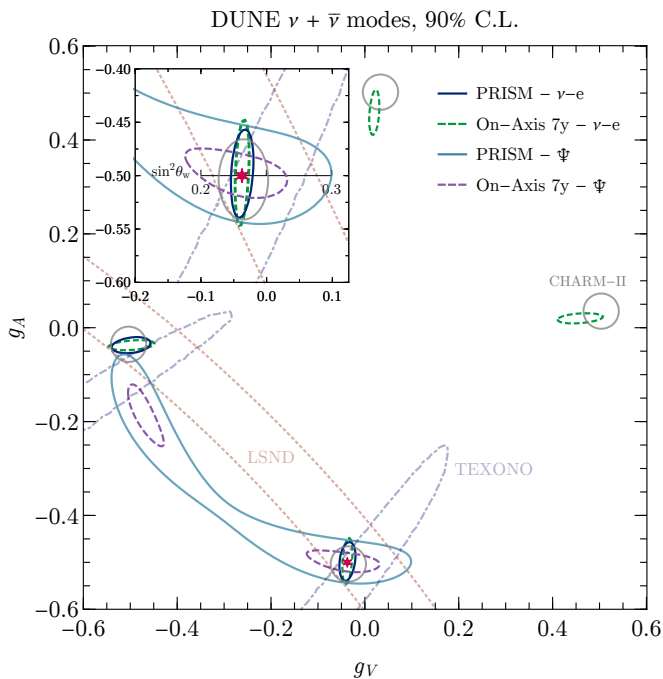


FIG. 2. Allowed regions in the plane  $g_V \times g_A$  from CHARM-II [39] (gray, at 90 %C.L.), LSND [40] (dotted light-brown, at  $1\sigma$  C.L.), and TEXONO [41] (dot-dashed light-violet, at  $1\sigma$  C.L.), and the estimated 90% C.L. sensitivity from on-axis DUNE electron scattering (dashed green) and tridents ( $\Psi$ ) (dashed purple), as well as DUNE-PRISM electron scattering (dark-blue) and tridents (light-blue), assuming the SM value indicated by the red star. For DUNE, we consider seven years of data-taking.

spectra of neutrino-electron scattering events for the first 5 off-axis positions. For each position, histograms corresponding to three pairs of vector and axial couplings ( $g_V, g_A$ ) are depicted:  $(-0.04, -0.5)$ , the SM expectation (solid);  $(-0.48, -0.04)$ , the leftmost degenerate region (dotted); and  $(0.47, 0.02)$ , the rightmost degeneracy is lifted due to the higher  $\nu_e$  composition of the flux, as depicted in Fig. 1. Error bars illustrating the statistical and systematic errors, are included for the SM case. DUNE-PRISM neutrino-electron scattering data, alone, cannot fully distinguish the SM from the leftmost degenerate region, as depicted in Fig. 2.

Neutrino-trident scattering, when a neutrino scatters off a nucleus giving rise to a charged lepton pair,  $\nu A \rightarrow \nu \ell^+ \ell^- A$ , where the leptons  $\ell$  can have the same or different flavors, is also sensitive to  $g_V$  and  $g_A$ .<sup>1</sup> This scattering can be coherent off the electromagnetic field of the nucleus or diffractive off the nucleons themselves. Although the trident cross section is quite involved (see

<sup>1</sup> Here we make the assumption that the electron and muon couplings to the  $Z$ -boson are identical.

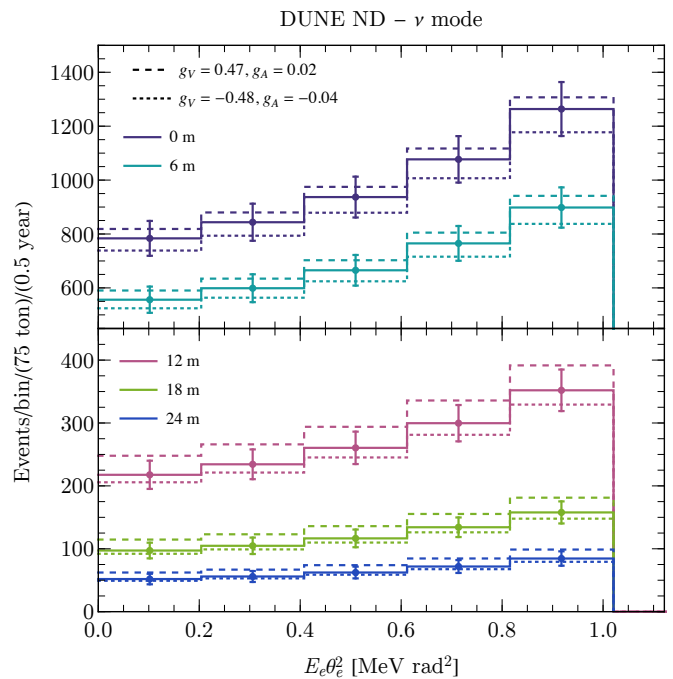


FIG. 3. Neutrino-electron event rates as a function of  $E_e \theta_e^2$  for the first 5 off-axis positions. For each position, the three histograms correspond to three pairs of vector and axial couplings ( $g_V, g_A$ ):  $(-0.04, -0.5)$  (solid);  $(-0.48, -0.04)$  (dotted); and  $(0.47, 0.02)$  (dashed). Error bars illustrating the statistical and systematic errors, are included for the SM case (solid histogram).

e.g. Refs [44–46]), in the limit where the final state leptons are massless, it is proportional to the electroweak parameters ( $C_V^2 + C_A^2$ ). For a  $\nu_\mu$  beam, these couplings are [44, 45]

$$C_V = g_V \quad C_A = g_A \quad (e^+e^- \text{ trident}), \quad (6)$$

$$C_V = g_V + 1 \quad C_A = g_A + 1 \quad (\mu^+\mu^- \text{ trident}). \quad (7)$$

The processes that lead to  $\mu^\mp e^\pm$  tridents are pure-charged-current and do not contribute to this discussion. Hence, measurements of  $e^+e^- \nu_\mu$ -tridents – the statistically-dominant mode – constrain  $g_V^2 + g_A^2$  while those of  $\mu^+\mu^- \nu_\mu$ -tridents constrain  $(g_V + 1)^2 + (g_A + 1)^2$  in the limit where the muon mass vanishes. A similar behavior is expected of  $\nu_e$ -tridents, with  $e \leftrightarrow \mu$ , and those associated to antineutrinos. It is easy to see that, in the limit where the muon mass vanishes, all cross sections are invariant under  $g_V \leftrightarrow g_A$ . A finite muon mass, however, breaks the  $g_V \leftrightarrow g_A$  symmetry.

Due to the very high intensity of the DUNE neutrino beam, this rare process is accessible. Fig. 2 also depicts the measurement of  $(g_V, g_A)$  from both  $\mu^+\mu^-$  and  $e^+e^-$  neutrino-trident events in DUNE on-axis (dashed purple) and DUNE-PRISM (light-blue), making use of the efficiencies estimated in [45]. Improvements on the reconstruction of di-electron or di-muon events would improve

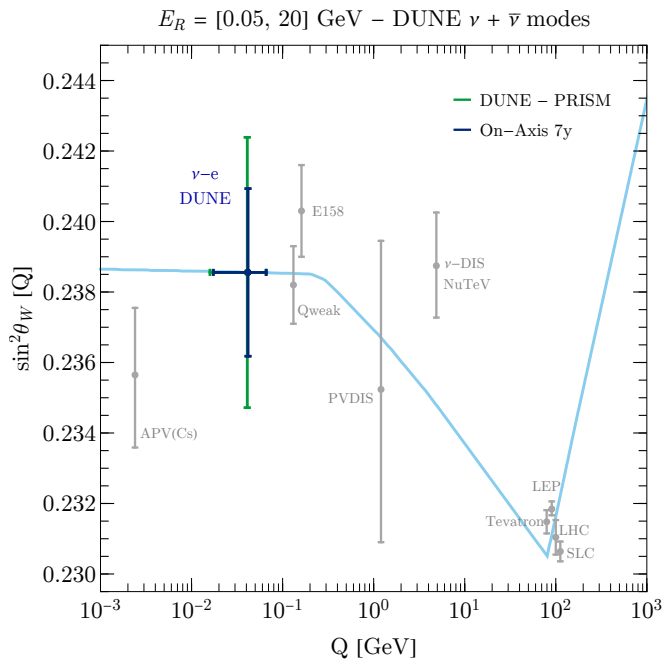


FIG. 4.  $\sin^2 \theta_W$  in the  $\overline{\text{MS}}$  scheme (light blue line) as a function of  $Q$ , obtained from a fit to existing data (gray data points), together with the DUNE on-axis (dark blue data point) and DUNE-PRISM (green data point) sensitivities to this angle. The horizontal error bars indicate the range of  $Q$  values accessible to DUNE neutrino-electron scattering. Note that the Tevatron, LHC and SLC data points were slightly shifted from  $Q = M_Z$  to improve readability.

the determination of the  $(g_V, g_A)$  couplings. The allowed region is not symmetric under  $g_V \leftrightarrow g_A$  since, as highlighted earlier, for DUNE energies, the mass of the muon is not negligible. Indeed, we checked that the subleading  $\mu^+ \mu^-$  neutrino-trident event sample plays the decisive role here. Hence, the combination of neutrino-electron scattering and neutrino trident data in the DUNE near detector complex, assuming these are consistent with the SM, lifts all degeneracies in the  $g_V \times g_A$  plane even if one chooses to exclude information from outside data.

Assuming the SM, our results can be translated into a measurement of  $\sin^2 \theta_W$  at  $\langle Q^2 \rangle = (40 \text{ MeV})^2$ . Fig. 4 depicts the value of  $\sin^2 \theta_W$  in the  $\overline{\text{MS}}$  scheme as a function of  $Q$ , obtained from a fit to existing data, together with our estimate for the expected DUNE and DUNE-PRISM sensitivities. The former is slightly better than the latter, but we emphasize that the on-axis measurement of  $\sin^2 \theta_W$  depends more strongly on the neutrino-flux modeling, while the DUNE-PRISM sensitivity depends more on the relative on- to off-axis flux uncertainties. Regardless, both measurements are estimated to be competitive with existing results.

In summary, we estimated that the future DUNE experiment will have excellent sensitivity to the vector and axial couplings of the electron to the  $Z$ -boson, and thus

to the weak mixing angle  $\sin^2 \theta_W$ , via precision measurements of neutrino-electron scattering. The sub-dominant  $\nu_e$  beam component in DUNE-PRISM, as well as neutrino trident events, play an important role in resolving degeneracies currently present in the world data.

We are extremely grateful to Luke Pickering for providing us with the flux covariance matrix, and we thank Laura Fields for useful discussions. The work of AdG is supported in part by the DOE Office of Science award #DE-SC0010143. This manuscript has been authored by Fermi Research Alliance, LLC under Contract No. DE-AC02-07CH11359 with the U.S. Department of Energy, Office of Science, Office of High Energy Physics. ZT is supported by Fundação de Amparo à Pesquisa do Estado de São Paulo (FAPESP) under contract 2018/21745-8.

- 
- [1] J. Erler and M. J. Ramsey-Musolf, *Phys. Rev.* **D72**, 073003 (2005), [arXiv:hep-ph/0409169 \[hep-ph\]](#).
  - [2] J. Erler and R. Ferro-Hernández, *JHEP* **03**, 196 (2018), [arXiv:1712.09146 \[hep-ph\]](#).
  - [3] M. Tanabashi *et al.* (Particle Data Group), *Phys. Rev.* **D98**, 030001 (2018).
  - [4] G. P. Zeller *et al.* (NuTeV), *Phys. Rev. Lett.* **88**, 091802 (2002), [Erratum: *Phys. Rev. Lett.* 90, 239902 (2003)], [arXiv:hep-ex/0110059 \[hep-ex\]](#).
  - [5] S. Schael *et al.* (ALEPH, DELPHI, L3, OPAL, SLD, LEP Electroweak Working Group, SLD Electroweak Group, SLD Heavy Flavour Group), *Phys. Rept.* **427**, 257 (2006), [arXiv:hep-ex/0509008 \[hep-ex\]](#).
  - [6] J. Pumplin, D. R. Stump, J. Huston, H. L. Lai, P. M. Nadolsky, and W. K. Tung, *JHEP* **07**, 012 (2002), [arXiv:hep-ph/0201195 \[hep-ph\]](#).
  - [7] S. Kretzer, F. Olness, J. Pumplin, D. Stump, W.-K. Tung, and M. H. Reno, *Phys. Rev. Lett.* **93**, 041802 (2004), [arXiv:hep-ph/0312322 \[hep-ph\]](#).
  - [8] E. Sather, *Phys. Lett.* **B274**, 433 (1992).
  - [9] E. N. Rodionov, A. W. Thomas, and J. T. Londergan, *Mod. Phys. Lett.* **A9**, 1799 (1994).
  - [10] A. D. Martin, R. G. Roberts, W. J. Stirling, and R. S. Thorne, *Eur. Phys. J.* **C35**, 325 (2004), [arXiv:hep-ph/0308087 \[hep-ph\]](#).
  - [11] J. T. Londergan and A. W. Thomas, *Phys. Rev.* **D67**, 111901 (2003), [arXiv:hep-ph/0303155 \[hep-ph\]](#).
  - [12] W. Bentz, I. C. Cloet, J. T. Londergan, and A. W. Thomas, *Phys. Lett.* **B693**, 462 (2010), [arXiv:0908.3198 \[nucl-th\]](#).
  - [13] M. Gluck, P. Jimenez-Delgado, and E. Reya, *Phys. Rev. Lett.* **95**, 022002 (2005), [arXiv:hep-ph/0503103 \[hep-ph\]](#).
  - [14] S. Kumano, *Phys. Rev.* **D66**, 111301 (2002), [arXiv:hep-ph/0209200 \[hep-ph\]](#).
  - [15] S. A. Kulagin, *Phys. Rev.* **D67**, 091301 (2003), [arXiv:hep-ph/0301045 \[hep-ph\]](#).
  - [16] S. J. Brodsky, I. Schmidt, and J.-J. Yang, *Phys. Rev.* **D70**, 116003 (2004), [arXiv:hep-ph/0409279 \[hep-ph\]](#).
  - [17] M. Hirai, S. Kumano, and T. H. Nagai, *Phys. Rev.* **D71**, 113007 (2005), [arXiv:hep-ph/0412284 \[hep-ph\]](#).
  - [18] G. A. Miller and A. W. Thomas, *Int. J. Mod. Phys.* **A20**,

- 95 (2005), [arXiv:hep-ex/0204007 \[hep-ex\]](#).
- [19] I. C. Cloet, W. Bentz, and A. W. Thomas, *Phys. Rev. Lett.* **102**, 252301 (2009), [arXiv:0901.3559 \[nucl-th\]](#).
- [20] K. P. O. Diener, S. Dittmaier, and W. Hollik, *Phys. Rev. D* **69**, 073005 (2004), [arXiv:hep-ph/0310364 \[hep-ph\]](#).
- [21] A. B. Arbuzov, D. Yu. Bardin, and L. V. Kalinovskaya, *JHEP* **06**, 078 (2005), [arXiv:hep-ph/0407203 \[hep-ph\]](#).
- [22] K. Park, U. Baur, and D. Wackerroth, in *Particles and fields. Proceedings, Meeting of the Division of the American Physical Society, DPF 2009, Detroit, USA, July 26-31, 2009* (2009) [arXiv:0910.5013 \[hep-ph\]](#).
- [23] K. P. O. Diener, S. Dittmaier, and W. Hollik, *Phys. Rev. D* **72**, 093002 (2005), [arXiv:hep-ph/0509084 \[hep-ph\]](#).
- [24] B. A. Dobrescu and R. K. Ellis, *Phys. Rev. D* **69**, 114014 (2004), [arXiv:hep-ph/0310154 \[hep-ph\]](#).
- [25] R. Acciarri *et al.* (DUNE), (2015), [arXiv:1512.06148 \[physics.ins-det\]](#).
- [26] K. Abe *et al.*, (2011), [arXiv:1109.3262 \[hep-ex\]](#).
- [27] L. Alvarez-Ruso *et al.*, *Prog. Part. Nucl. Phys.* **100**, 1 (2018), [arXiv:1706.03621 \[hep-ph\]](#).
- [28] J. M. Conrad, J. M. Link, and M. H. Shaevitz, *Phys. Rev. D* **71**, 073013 (2005), [arXiv:hep-ex/0403048 \[hep-ex\]](#).
- [29] A. de Gouvêa and J. Jenkins, *Phys. Rev. D* **74**, 033004 (2006), [arXiv:hep-ph/0603036 \[hep-ph\]](#).
- [30] S. K. Agarwalla and P. Huber, *JHEP* **08**, 059 (2011), [arXiv:1005.1254 \[hep-ph\]](#).
- [31] J. M. Conrad, M. H. Shaevitz, I. Shimizu, J. Spitz, M. Touns, and L. Winslow, *Phys. Rev. D* **89**, 072010 (2014), [arXiv:1307.5081 \[hep-ex\]](#).
- [32] A. Adelman, J. Alonso, W. A. Barletta, J. M. Conrad, M. H. Shaevitz, J. Spitz, M. Touns, and L. A. Winslow, *Adv. High Energy Phys.* **2014**, 347097 (2014), [arXiv:1307.6465 \[physics.acc-ph\]](#).
- [33] O. Tomalak and R. J. Hill, (2019), [arXiv:1907.03379 \[hep-ph\]](#).
- [34] R. J. Hill and O. Tomalak, (2019), [arXiv:1911.01493 \[hep-ph\]](#).
- [35] K. Abe *et al.* (T2K), *Phys. Rev. D* **87**, 012001 (2013), [Addendum: *Phys. Rev. D* **87**, no.1, 019902(2013)], [arXiv:1211.0469 \[hep-ex\]](#).
- [36] L. Aliaga *et al.* (MINERvA), *Phys. Rev. D* **94**, 092005 (2016), [Addendum: *Phys. Rev. D* **95**, no.3, 039903(2017)], [arXiv:1607.00704 \[hep-ex\]](#).
- [37] C. M. Marshall, K. S. McFarland, and C. Wilkinson, (2019), [arXiv:1910.10996 \[hep-ex\]](#).
- [38] L. Pickering, “DUNE-PRISM analysis update,” (2019), DUNE collaboration meeting.
- [39] P. Vilain *et al.* (CHARM-II), *Phys. Lett. B* **335**, 246 (1994).
- [40] L. B. Auerbach *et al.* (LSND), *Phys. Rev. D* **63**, 112001 (2001), [arXiv:hep-ex/0101039 \[hep-ex\]](#).
- [41] M. Deniz *et al.* (TEXONO), *Phys. Rev. D* **81**, 072001 (2010), [arXiv:0911.1597 \[hep-ex\]](#).
- [42] M. Carena, A. de Gouvêa, A. Freitas, and M. Schmitt, *Phys. Rev. D* **68**, 113007 (2003), [arXiv:hep-ph/0308053 \[hep-ph\]](#).
- [43] L. Pickering, Private communication.
- [44] G. Magill and R. Plestid, *Phys. Rev. D* **95**, 073004 (2017), [arXiv:1612.05642 \[hep-ph\]](#).
- [45] P. Ballett, M. Hostert, S. Pascoli, Y. F. Perez-Gonzalez, Z. Tabrizi, and R. Zukanovich Funchal, *JHEP* **01**, 119 (2019), [arXiv:1807.10973 \[hep-ph\]](#).
- [46] W. Altmannshofer, S. Gori, J. Martín-Albo, A. Sousa, and M. Wallbank, (2019), [arXiv:1902.06765 \[hep-ph\]](#).